tvst

Special Issue

In Vivo Subretinal ARPE-19 Cell Tracking Using Indocyanine Green Contrast-Enhanced Multimodality Photoacoustic Microscopy, Optical Coherence Tomography, and Fluorescence Imaging for Regenerative Medicine

Van Phuc Nguyen[1], Yanxiu Li[1], Jessica Henry[1], Thomas Qian[1], Wei Zhang[2], Xueding Wang[2], and Yannis M. Paulus[1,2]

[1] Department of Ophthalmology and Visual Sciences, University of Michigan, Ann Arbor, MI, USA
[2] Department of Biomedical Engineering, University of Michigan, Ann Arbor, MI, USA

Correspondence: Yannis M. Paulus, Department of Ophthalmology and Visual Sciences, Department of Biomedical Engineering, University of Michigan, 1000 Wall Street, Ann Arbor, MI 48105, USA.
e-mail: ypaulus@med.umich.edu

Received: January 31, 2021
Accepted: July 5, 2021
Published: September 2, 2021

Keywords: cells tracking; photoacoustics microscopy; optical coherence tomography; regenerative medicine; contrast agents

Citation: Nguyen VP, Li Y, Henry J, Qian T, Zhang W, Wang X, Paulus YM. In vivo subretinal ARPE-19 cell tracking using indocyanine green contrast-enhanced multimodality photoacoustic microscopy, optical coherence tomography, and fluorescence imaging for regenerative medicine. Transl Vis Sci Technol. 2021;10(10):10, https://doi.org/10.1167/tvst.10.10.10

Purpose: Cell-based regenerative therapies are being investigated as a novel treatment method to treat currently incurable eye diseases, such as geographic atrophy in macular degeneration. Photoacoustic imaging is a promising technology which can visualize transplanted stem cells in vivo longitudinally over time in the retina. In this study, a US Food and Drug Administration (FDA)-approved indocyanine green (ICG) contrast agent is used for labeling and tracking cell distribution and viability using multimodal photoacoustic microscopy (PAM), optical coherence tomography (OCT), and fluorescence imaging.

Methods: Twelve rabbits (2.4–3.4 kg weight, 2–4 months old) were used in the study. Human retinal pigment epithelial cells (ARPE-19) were labeled with ICG dye and transplanted in the subretinal space in the rabbits. Longitudinal PAM, OCT, and fluorescence imaging was performed for up to 28 days following subretinal administration of ARPE-19 cells.

Results: Cell migration location, viability, and cell layer thickness were clearly recognized and determined from the fluorescence, OCT, and PAM signal. The in vivo results demonstrated that fluorescence signal increased 37-fold and PAM signal enhanced 20-fold post transplantation.

Conclusions: This study demonstrates that ICG-assisted PAM, OCT, and fluorescence imaging can provide a unique platform for tracking ARPE-19 cells longitudinally with high resolution and high image contrast.

Translational Relevance: Multimodal PAM, OCT, and fluorescence in vivo imaging with ICG can improve our understanding of the fate, distribution, and function of regenerative cell therapies over time nondestructively.

Introduction

Stem cell-based therapeutics potentially provide a permanent replacement of degenerated tissues and cells[1] in conditions including cancer, diabetes, and ocular diseases.[1–5] The need for effective cell-based regenerative medicine therapies (RMTs) in the field of ophthalmology is of particular interest due to the growing elderly population experiencing vision loss.[6] RMTs broadly include cell-based therapies like stem cells, stromal cells, and progenitor cells. The eye, in particular the retinal pigment epithelium (RPE), is an ideal application of RMTs due to the accessibility and distinct margins of the eye and the ability to monitor transplantation directly in vivo

with high resolution optical imaging.[7] The RPE is a pigmented cell monolayer between the neurosensory retina and vascular choroid and forms a part of the blood-retina barrier. The thin layer is necessary and important for vision because it maintains the retinoid cycle for phototransduction, sustains photoreceptor functionality, and protects the retina against solar radiation.[8] The RPE in some disease states, like geographic atrophy from age-related macular degeneration (AMD), is unable to adequately repair itself. This can lead to vision threatening diseases and blindness. RMTs, including stem cell-derived retinal cell therapies, serve as a potential method of regenerating injured RPE and restoring vision given their ability to replace and restore RPE via transplantation, proliferation, and cell differentiation.[8]

Potential methods of treating AMD caused by RPE degeneration are stem cell therapies and drug-based therapies. The RPE is particularly complex to develop therapeutics for treatment due to the blood-retinal barrier limiting the access of drugs and xenobiotics to the cells.[9] The melanin produced in the RPE additionally affects the pharmacokinetics due to the protein's tendency to accumulate and bind to therapeutics.[10–13] This accumulation and binding can lead to reduced peak responses of drugs and prolonged drug action, which complicates the reliability of the drug dosage and efficacy.[14,15] For these reasons, cell-based therapeutics are preferred in the treatment of RPE-based ocular diseases. The developing field of RMTs in ophthalmology has not yet established an effective therapeutic approach to treat the degradation of the RPE and other retinal structures. There are many clinical trials underway for stem cell therapy on the retina that are performed by translocation of RPE cells via subretinal injection.[16,17] A clinical trial in 2014 by Schwartz et al. demonstrated improved visual acuity in patients who received human embryonic stem-cell (hESC)-derived RPE cells for the RPE and failed to show any toxicity or longevity concerns.[18,19] These RMT methods can improve the health of the photoreceptors.[20] However, limitations exist for these techniques. There are possible risks, including tumor formation, immune reactions, efficacy concerns, and a general lack of understanding of the mechanism of action.[21] These risks could be addressed through adequate imaging and assays; however, the majority of these clinical trials rely on histopathological image analysis to comprehensively understand the fate of the transplanted cells in their migration, survival, and function over time in vivo.[22] This method is highly invasive and difficult or impossible to execute in in vivo models. For this reason, it can be difficult to acquire convincing safety and efficacy data. A potential solution to this barrier is the use of noninvasive, high-resolution imaging techniques and contrast agents.

Many imaging modalities have been investigated for the analysis of RPE cell therapies. Some prominent methods of clinical imaging include magnetic resonance imaging (MRI), positron emission tomography (PET), single photon emission computed tomography (SPECT), bioluminescence, fluorescence microscopy, and two-photon fluorescence imaging.[23,24] These technologies have become more sophisticated in recent years and have the capacity to noninvasively perform analysis of transplanted cells and cell therapies.[23] However, they still have limitations, including the high-cost and ionizing radiation-associated risk seen in PET and SPECT. Bioluminescence provides real-time imaging but lacks spatial resolution to track cell movement. Fluorescence microscopy has the advantage of high sensitivity but lacks depth of penetration.[25] Although two-photon fluorescence imaging has better penetration depth in tissue (500 µm to 1 mm) and less photobleaching and phototoxicity to the cells than conventional fluorescence imaging, this imaging modality requires expensive, specialized lasers and equipment.[24]

Photoacoustic imaging is a unique solution that utilizes acoustic waves produced by thermal expansion of a tissue after a short duration laser pulse. The system has demonstrated a depth of penetration of several centimeters, submillimeter spatial resolution, and rapid temporal resolution.[26] This technology can be synergistically combined with other imaging modalities, including scanning laser ophthalmoscopy (SLO), fluorescence microscopy, and optical coherence tomography (OCT), and also exogenous contrast agents. This investigation presents a novel multimodal photoacoustic microscopy (PAM), OCT, and fluorescence imaging systems to longitudinally monitor cells transplanted into the subretinal space. PAM uses a nanosecond pulsed duration laser to convert light to sound to produce a PA signal. This produces a high-resolution, high-contrast image from the optical absorption of light at 10 mm depths. OCT provides additional information by evaluating scattering effects and low-coherence interferometry to provide structural information of the retinal layers. The OCT system can also be used for real-time image-guided subretinal injection,[26,27] which makes the multimodal PAM and OCT imaging systems ideal for optical RMTs.

Exogenous contrast agents can be a valuable resource to distinguish stem cells from endogenous tissues. The improved sensitivity can be provided by nanoparticles and organic chromophores with PAM and OCT imaging.[28] The two categories of

contrast agents for improved visualization of biological tissues include organic and inorganic materials. Inorganic PA contrast agents include gold nanoparticles, silica,[29,30] copper sulfide nanoparticles,[31] and carbon nanotubes.[32] Although these are valuable methods of improving contrast, they possess long-term toxicity concerns and have not been approved at this time by the US Food and Drug Administration (FDA) for clinical use. Organic contrast agents, most notably indocyanine green (ICG), have demonstrated excellent biodegradability and biocompatibility for PA imaging in vivo.[33–35] This near-infrared FDA approved dye has shown high optical absorption and high PA contrast in tumors in vivo.[36] ICG can be used to label stem cells that are injected into the subretinal space to repair damaged RPE. For this reason, it will be a key focus of this investigation due to its potential for rapid clinical translation.

This research examines the potential usage of ICG-labeled adult retinal pigment epithelial cell line 19 (ARPE-19) and multimodal PAM, OCT, and fluorescence imaging as a potential treatment and real-time assay method for RPE damage. The ICG contrast dye paired with the in vivo multimodal PAM and OCT imaging system can track the longevity and movement of the ARPE-19 cells. To investigate the hypothesis, the ICG-ARPE-19 cells are injected subretinally in rabbits using real-time OCT image guidance. These rabbits are visualized over a period of 3 months following the injections using PAM, OCT, and fluorescence to monitor regeneration and migration for RMTs like ARPE-19 cells.

Materials and Methods

Cell Culture

Human retinal pigment epithelial cells with differentiated properties (ARPE-19) were prepared. ARPE-19 cells were cultured in DMEM/F12 medium augmented 100-mm tissue culture dishes with 15 mM HEPEs (Sigma, St. Louis, MO, USA), L-glutamine, 10% fetal bovine serum, 1.16 g/L sodium bicarbonate, and antibiotic-antimycotic. Cells were grown in a humidified incubator at 37°C and 5% CO_2 and 95% air. When the cells were deemed 70 to 90% confluent, they were isolated through the addition of 1 mL of 0.25% trypsin-EDTA and then centrifuged at 500 rpm for 5 minutes. The human ARPE-19 cells were generously donated by Dr. David A. Antonetti at the University of Michigan.

In Vitro Toxicity and Biodegradable of ICG

Methyl tetrazolium (MTT) assay was conducted to determine potential cytotoxicity of ICG on the ARPE-19 cells. The ARPE-19 cells were seeded in 96-well plates at a density of 10^4 cells/well and incubated for 24 hours at 37°C and 5% CO_2. ICG contrast agent was added to the cells at various concentrations (0 [control], 12.5, 25, 50, 100, 200, 400, and 500 µg/mL). For biodegradable testing, cells were cultured with ICG at a final concentration of 200 µg/mL in medium followed by laser illumination at different fluences (i.e. 0.0025, 0.005, 0.01, 0.02, and 0.04 mJ/cm^2). The cells were then incubated for 24 and 48 hours. Afterward, the standard MTT assay was used to determine the percentage of cells viable. Briefly, treated cells were washed with cold PBS and then 100 µL MTT reagent (1 mg/mL) in medium was added into the cells, covered with foil, and incubated in the dark for 4 hours at 37°C. When mitochondrial succinate dehydrogenase in live cells transformed MTT into visible purple formazan crystals that were observed under a microscope, 100 µL of DMSO was added into the cells to dissolve the formazan crystal. The samples were then kept at room temperature for 20 minutes. Optical density (OD) was measured at the wavelength of 570 nm using Epoch micro-plate reader (BioTek, Winooski, VT, USA). The relative survival rate of the transplanted cell was calculated and compared with that of control group without treated with ICG using the following formula:

$$P = \frac{\text{OD experimental group}}{\text{OD control group}} \times 100 \qquad (1)$$

The additional measures of apoptosis, cell viability, and cell death were quantified using flow cytometry analysis carried out by Annexin-V FITC Apoptosis Detection Kit (BD Biosciences, San Jose, CA, USA). The ARPE-19 cells were incubated with ICG at a final concentration of 250 µg/mL in medium for 24 hours and 48 hours. The cells were then harvested and resuspended in mixed 500 µL 1× buffer binding with 5 µL (10 µg/mL) of Annexin V FITC and PI solution at room temperature and without light exposure for 15 minutes. Then, 1 mL PBS suspension was added to the stained cells for flow cytometer analysis.

Cellular Uptake

The quantity of ICG uptake was observed and evaluated using confocal microscopy. The cells were grown in 35 mm µ-plates at a density of 2 ×

10^5 cells/well and incubated at 37°C and 5% CO_2 for 24 hours. The sterile ICG was introduced to the ARPE-19 cells at different concentrations of 150, 200, and 250 µg/mL and incubated for 24 hours. The treated ARPE-19 cells were rinsed with cold PBS 3 times and fixed with 2.5 % formaldehyde for 30 minutes. The fixed ARPE-19 cells were stained with DAPI (300 µL, 10 µg/mL) for 20 minutes. The samples were then finally washed with PBS two more times. A confocal microscope SP5 was used to monitor the uptake and distribution of ICG (SP5; Leica Microsystems Inc., Buffalo Grove, IL, USA).

PAM/OCT Imaging of ICG-labeled ARPE-19 Cells In Vitro

The optical properties of ICG were analyzed and evaluated. The absorption spectrum of ICG was determined from 350 to 1000 nm by ultraviolet-visible (UV-Vis) spectroscopy (UV-3600; Shimadzu Corp., Kyoto, Japan) to determine the ideal excitation wavelength for PAM imaging.

PAM imaging was used for single cell detection through imaging fixed samples of ARPE-19 cells labeled with ICG at different concentrations of 150, 200, and 250 µg/mL and incubated for 24 hours. The samples were individually scanned using an area of 0.2 × 0.2 mm^2 at 700 nm with a laser energy of 40 nJ, respectively. The average PA amplitudes that surpassed the background level versus the quantity of cells was measured and plotted.

Preparation for ARPE-19 Cells With ICG for In Vivo Subretinal Injection

ARPE-19 cells were labeled with ICG at a final concentration of 250 µg/mL in nutritional media and incubated for 24 hours. The cells were next rinsed with cold PBS three times to aspirate any ICG remaining in solution. The ICG-tagged ARPE-19 cells were harvested using 0.05% Trypsin/EDTA and then centrifuged, counted, and resuspended in 100 µL of cold PBS. The cell density was determined using an automatic cell reader.

To prepare dead ARPE-19 cells, the harvested ARPE-19 cells were treated with laser at power of 500 mW, pulsed duration of 0.5 seconds, laser spot size of 500 µm using the Vitra 532 nm Photocoagulator (Quantel Medical, Cournon d'Auvergne, France). Then, 100 µL of the treated cells were stained with Trypan blue to count the percentage of dead cells.

In Vivo Subretinal Injection of ARPE-19 Cells

All rabbits under anesthesia received subretinal injection of ICG-labeled ARPE-19 cells. The rabbit head was placed under a dissecting microscope and the head positioned onto its side so that the eye that was to be injected was facing the ceiling. Then, a localized peritomy was performed, and the superior rectus muscle was removed using scissors. A sclerotomy approximately 3.5 to 4 mm posterior to the limbus was created using a 26 G sharp disposable pre-sterilized needle. The needle was placed at an angle to avoid touching the lens with the needle given the larger relative size of the lens in the rabbit eye. A contact lens coupled with Gonak gel was placed on the retina. The tip of the syringe containing ARPE-19 cells with the 30 G needle was inserted through the hole and gently advanced through the eye until observing the needle tip approach the retinal tissue under the operating microscope. After visualization of the needle in the subretinal space, careful injection of the ARPE-19 cells was slowly performed into the subretinal space. Finally, the syringe was retracted slowly, and the retina was monitored with different imaging modalities. To minimize immunosuppression in animals to save transplanted cells, a dose of triamcinolone 2 mg (100 µL) was intravitreally injected into the rabbit eye 1 week before subretinal transplantation (Triescence; Alcon Nordic) as described previously by Petrus-Reurer et al.[37] and Reyes et al.[20]

Multimodality PAM, OCT, and Fluorescence Imaging Equipment

The PAM system light source involves a tunable excitation nanosecond pulsed laser light (3–5 ns) with a pulse repetition rate of 1 kHz pumped by diode solid-state laser (NT-242; Ekspla, Vilnius, Lithuania). The PA excitation beam incidence is circular shaped with an estimated diameter of 2 mm and the wavelength can be adjusted from 405 to 2600 nm. The fluence on the retina was 80 nJ at 570 nm, respectively, which is half of the American National Standards Institute (ANSI) safety limit for the eye, which avoids damage to the retina.[38,39] The scan area was determined to be 5 × 5 mm^2 and the resolution was 256 × 256 pixels. The axial and lateral resolutions were 4.1 and 37.0 µm. The image acquisition time was approximated at 65 seconds and limited by the 1 kHz pulse repetition rate of the tunable OPO laser. A custom-made needle-shaped ultrasound transducer with a central frequency of 27.0 MHz was used to detect the laser-induced acoustic signals. Amira software was used to analyze the PA image data obtained at two wavelengths through combining, reconstructing, and partitioning in

3D using (Visualization Sciences Group). The median PA signal within transplanted cells was assessed for each PA image, with the error bars demonstrating the standard deviation of measurements achieved in three different samples.

The spectral-domain OCT used in this investigation before, during, and after injection of ARPE-19 cells was adapted from a commercially available OCT system (Ganymede-II-HR; Thorlabs, Newton, NJ). The system was modified through the addition of an ocular lens after the scan lens and a dispersion compensation glass in the reference arm.[40] Two super luminescent diodes with center excitation wavelengths of 846 nm and 932 nm were used to induce OCT signals and illuminate the samples. The resolutions of the axial and lateral OCT were determined using the full width at half-maximum (FWHM) and found to be 4.0 and 3.8 μm, respectively. The OCT and PAM excitation beams of incident were coaxially aligned so that OCT could guide and aid in the interpretation of PAM results.

Color Fundus Photography, Fluorescence Imaging, and Slit Lamp Examination Follow Up

All the rabbits before and after subretinal injection of ICG labeled ARPE-19 cells were imaged with color fundus photography and ICGA and received slit lamp biomicroscopy. The fundus color images were obtained using TOPCON system (Topcon 50EX; Topcon Corporation, Tokyo, Japan). All the color fundus images were acquired using the same exposure parameters (Iso = 50, flash = 18, and image type = daylight). The fluorescence imaging was also achieved using Topcon 50EX system. However, internal excitation and emission filter sets were applied when switching to fluorescent imaging module. The fluorescence images were acquired before and after subretinal delivery of labeled ARPE-19 cells before and after the photoacoustic imaging session. Slit lamp biomicroscopy examination was performed using a Zeiss SL120, Carl Zeiss, Germany, slit lamp to perform a full dilated ophthalmic examination to evaluate for evidence of rejection, inflammation, cataract, or other pathology.

In Vitro and In Vivo Multimodal High-Resolution PAM and OCT Imaging

In vivo PAM and OCT provides multimodal, high resolution image acquisition as detailed in previous a previous investigation.[41] All animal experiments were in accordance with the guidelines of the Association for Research in Vision and Ophthalmology (ARVO) Statement on the care and use of laboratory animals in Ophthalmic and Vision Research after the protocol was approved by the Institutional Animal Care and Use Committee (IACUC) at the University of Michigan (PRO00008566). White New Zealand rabbits were generously donated by the Center for Advanced Models and Translational Sciences and Therapeutics (CAMTraST) at the University of Michigan Medical School.

Twelve rabbits ranging from 2.4 to 3.4 kg and aged 2 to 4 months old were used in the study and randomly divided into 4 groups ($N = 3$ for each group): 3 received subretinal injection of ICG-ARPE-19 suspension, 3 received subretinal injection of ICG solution at concentration of 20 μg/mL, 3 received subretinal injection of dead ICG-ARPE-19 suspension, and 3 served as the control group. The control group received subretinal injection of balanced salt solution (BSS).

The experimental group was first anesthetized with xylazine and ketamine. The 1% tropicamide ophthalmic and 2.5% phenylephrine hydrochloride solution were used to dilate the pupils of each rabbit. Five minutes before imaging, 0.5% topical tetracaine was administered in each eye for topical anesthesia of the cornea. The rabbits then received subretinal injection of 30 μL of ICG-labeled ARPE-19 cells at a density of 1×10^6 cells per millimeter. Both the OCT and microscope were used in real-time to guide the injection of the solution into the subretinal space. Transplanted cells were imaged with multimodality imaging, including color fundus photography, fluorescein angiography (FA), ICG fluorescence imaging, PAM, and OCT to monitor the migration and distribution of the transplanted ARPE-19 cells as well as any structural changes to the retinal blood vessels. To perform multimodal PAM and OCT imaging, the rabbit's eyes were positioned at the center of the scan area, and the rabbit's bodies were placed on a stabilizing platform to minimize motion artifacts. Sterile saline was applied to the cornea every 42 to 60 seconds to prevent corneal dehydration and provide acoustic coupling between the conjunctiva and the ultrasound transducer. A water circulating heating blanket was placed under the rabbit to maintain body temperature throughout the experiment. The 0.75% isoflurane and O_2 (1 L/min) were provided for appropriate anesthesia. Respiration rate, heart rate, and rectal body temperature were monitored and documented every 15 minutes.

Immunostaining and Histological Analysis

To assess the movement and interaction of the ARPE-19 ICG cells with the native RPE cells after

injection, immunohistochemistry staining was first performed with the primary RPE65 antibody (Abcam ab78036, clone [401.8B11.3D9]). The RPE65 antibody was diluted 1:200 in mixed solution of Dulbecco's PBS (DPBS), 4% FBS and 0.1% Tween-20 for 24 hours at 4°C. This was repeated with secondary Alexa Fluor 555 donkey anti-rabbit IgG (1:1000; Life Technologies, A31572) and Alexa Fluor 647 anti-mouse IgG antibodies (1:1000; Life Technologies, A31571) in DPBS solution with 4% FBS, 0.1% Tween-20 and incubated for 2 hours at room temperature. Prolonged gold mounting medium with DAPI (Vector Laboratories, Burlingame, CA, USA) was with 24 × 50 mm cover slip used to mount the slides. The samples were visualized using a light Leica microscope (DM6000; Leica Biosystems, Nussloch, Germany) and then captured with the Leica Application Suite software (LAS X; Leica Biosystems). Image processing and analysis were then conducted using ImageJ and Imaris software.

The rabbits were euthanized at day 28 by intravenous injection of euthanasia solution (0.22 mg/kg) (Beuthanasia-D Special; Intervet Inc., Madison, NJ, USA). The whole eye was removed and fixed in Davidson's fixative solution (Electron Microscope Sciences, Hatfield, PA, USA) for 24 hours at room temperature. The samples were then transferred to 50% alcohol solution (Thermo Fisher Scientific, Allentown, PA, USA) for 8 hours and 70% alcohol solution for 24 hours. The fixed samples were divided into 5 to 6 mm rectangular segments and embedded in paraffin. Leica autostainer XL (Leica Biosystems) was then used to section the segments into a thickness of 6 µm serially. The sectioned samples were stained with hematoxylin and eosin (H&E) for histopathological analysis.

Statistical Analysis

All the experiments were conducted and repeated at least three times in this study. The final data are displayed as the average ± standard deviation (SD). A Student *t*-test was performed to determine statistically significant variations between control and experimental groups. Any P values of < 0.05 were considered statistically significant.

Results and Discussions

In Vitro Characterization of ICG Contrast Agents

Figure 1A shows the absorption spectrum of ICG obtained from various concentrations (i.e. 0 [saline], 6.25, 12.5, 25, 50, and 100 µg/mL) using UV–Vis spectroscopy. The result illustrates the absorption peak of ICG at 850 nm and the optical absorption increases with concentration. To examine the optical properties with the change in bioenvironment, the absorption spectrum of internalized ICG inside ARPE-19 cells was measured. As shown in Figure 1B, the control cells without treatment with ICG showed low optical absorption. In contrast, the absorption spectrum of the internalized ICG reached a peak at 800 nm and 900 nm. This result is slightly different from the absorption spectrum of free ICG dye due to the accumulation of ICG inside the cells. In addition, the peak at 900 nm may allow for selecting longer excitation wavelength to obtain deeper information of the tissue in living animals. To test hypothetical photobleaching effect during longitudinal in vivo experiments, the photostability was implemented on the cells labeled with ICG samples by irradiation of the sample with laser light at 700 nm at different laser energies (i.e. 40, 80, 160, 320, and 640 nJ) and then the absorption spectrum of these samples was measured and plotted, as shown in Figure 1C. The absorption spectrum panel shows that the absorption fluctuates within 1 to 2%, indicating the photostability of the internalized ICG.

In Vitro Toxicity and Cellular Uptake Analysis

ARPE-19 is a common RPE cell line for study of different eye diseases, such as diabetic retinopathy due to its stable and retain differentiated properties.[42] Prior to performing transplantation of the cells into the subretinal space in the rabbit retina, biocompatibility of ICG was evaluated on ARPE-19 cells using different methods, such as MTT assay and flow cytometry analysis. Figure 1D exhibits the viability of ARPE-19 cells cultured with ICG suspension solution at various concentrations and incubation times. The ARPE-19 cells treated with blank medium (control group) shows no negative impact on cell viability for all treatment conditions. In comparison with the control group, the population of the treated cells with ICG also illustrates that the cell viability was not significantly decreased for most concentrations of ICG and incubation times. At the highest treated concentration, the cells without viability were reduced slightly from 4.83% to 5.98% compared to the control group (survival rate = 100% for control versus 95.16% and 94.01% for 24 hours and 48 hours at 500 µg/mL of ICG). This result confirms that ICG demonstrates great biocompatibility and is an excellent candidate for in vivo cell-based therapy applications.

To assess the potential of laser-induced singlet oxygen after being irradiated, cytotoxicity of the ICG labeled with ICG cells followed by laser illuminations

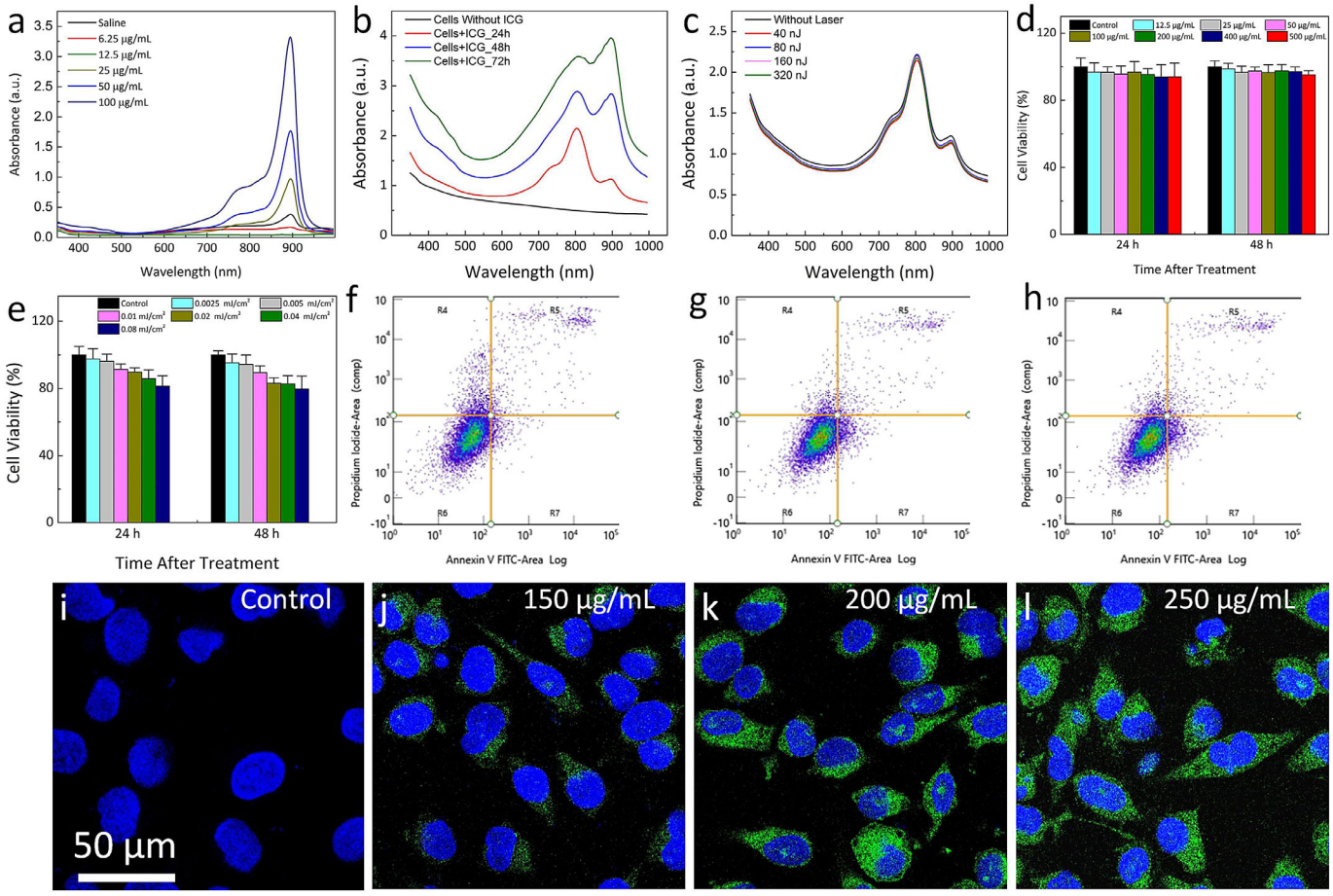

Figure 1. **Optical characterization, in vitro toxicity and cellular uptake of ICG.** (**A**) UV-Vis absorption spectrum of ICG dye obtained at various concentrations (i.e. 0 [saline], 6.25, 12.5, 25, 50, and 100 µg/mL). (**B**) UV-Vis absorption spectrum of ICG labeled ARPE-19 cells measured from the samples incubated with 250 µg/mL at 24 hours, 48 hours, and 72 hours. (**C**) Absorption spectra of the treated cells under laser illumination at various energies from 0 to 640 nJ, revealing photostability of the labeled cells. (**D**) Cytotoxicity of ICG in ARPE-19 cells. ICG at different concentrations ranging from 0 to 500 µg/mL was cultured with ARPE-19 cell at various time points: 24 hours and 48 hours. (**E**) Cell viability of ARPE-19 cells labeled with ICG at concentration of 200 µg/mL followed laser illumination at different laser fluences (i.e. 0.0025, 0.005, 0.01, 0.02, and 0.04 mJ/cm^2). (**F–H**) Flow cytometry analysis obtained from three groups: control group **D**, treated group with ICG at 250 µg/mL and incubated for 24 hours **E**, and 48 hours (**F**), $n = 3$, $P < 0.001$. (**I–L**) Confocal laser scanning macroscopic images of the internalized ICG inside the cells. ARPE-19 cells were cultured with ICG suspension solution at different concentrations (i.e. 0 [control], 150, 200, and 250 µg/mL) for 24 hours. Pseudo-green fluorescence color illustrates the distribution of internalized ICG inside the cells.

were evaluated, as shown in Figure 1E. This result shows that the laser induced mild impact on the cell viability post laser illumination. The percentage of cell survival is about 80% on the sample treated with laser at the highest fluence of 0.16 mJ/cm^2, illustrating that laser irradiation at this fluence may induce less singlet oxygen when compared to that of higher laser fluence irradiation, as described by Cardillo et al.[43]

The biocompatibility of ICG was further evaluated using the flow cytometry analysis. The flow cytometry analysis was implemented to assess the potential early apoptosis of the ARPE-19 cells. The cells were co-cultured with ICG at a final concentration of 200 µg/mL and incubated for 24 and 48 hours followed by apoptosis quantification using Annexin-V/PI detection kits (Figs. 1F, 1G). The treated samples with ICG suspension solution illustrate a slight apoptosis above the apoptosis level (total apoptosis [early and late apoptosis] = 7.5% for control, 8.69% for 24 hours, and 9.95% for 48 hours for ARPE-19 cells), demonstrating that ICG was not toxic to the human differentiated retinal cell lines at the tested concentration.

To observe the biodistribution activity of ICG inside the ARPE-19 cells, the intracellular uptake of ICG dye into the cells was observed using laser scanning confocal microscopy. Figure 1I–L shows the confocal microscopic images of the internalized ICG inside the cells at different concentration (i.e. 150,

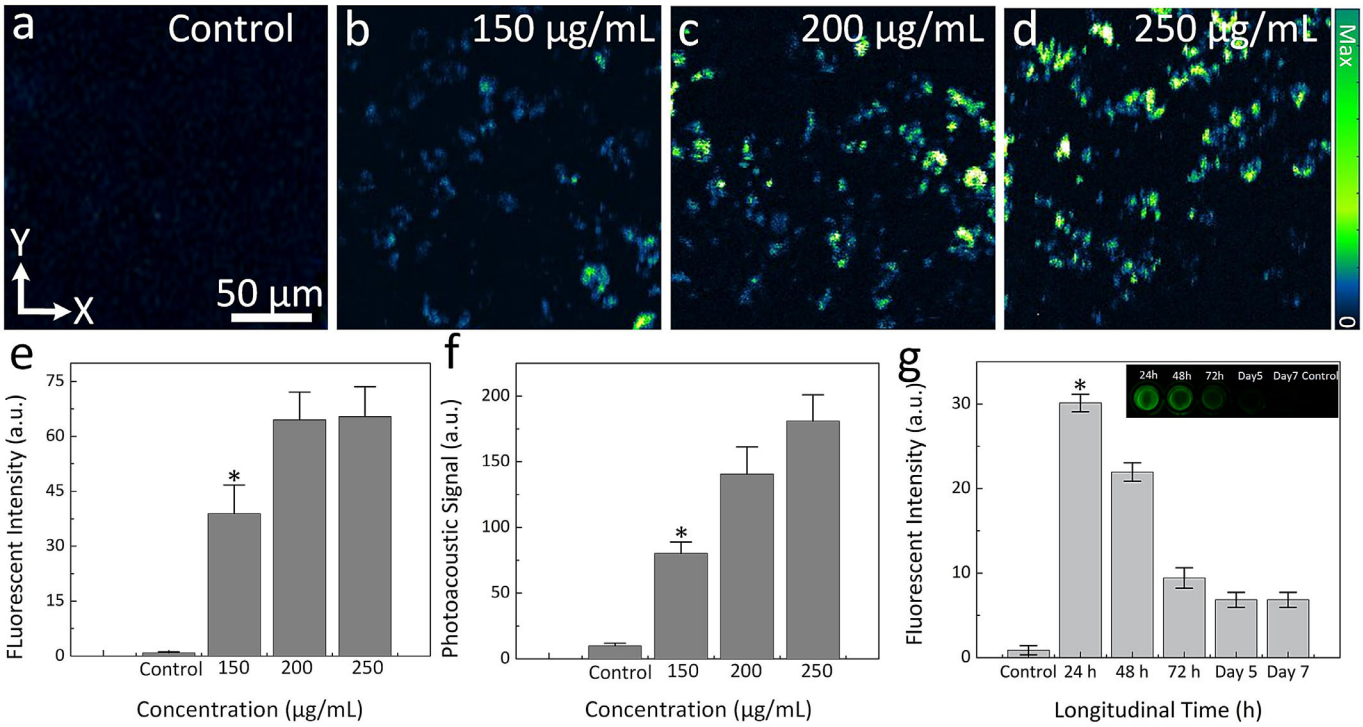

Figure 2. **In vitro photoacoustic microscopy of single ARPE-19 cells.** (**A–D**) In vitro PAM images of single ARPE-19 cells. The PAM images were obtained using the excitation wavelength of 700 nm and laser energy of 80 nJ. (**E**) Graph of fluorescent intensity as a function of concentrations. (**F**) Quantitative measurement of photoacoustic signal. (**G**) In vitro biodegradable of ICG dyes in bioenvironment. The fluorescent signal gradually reduced over time ($n = 5$, $P < 0.05$).

200, and 250 µg/mL). Pseudo-green color indicated the accumulation of ICG dye inside the cells whereas no evidence of green fluorescence color was observed in the control group (treated with blank medium). The ICG dye significantly increased uptake in the cells at a concentration of 200 and 250 µg/mL post treatment, whereas low fluorescence contrast was visible on the confocal image of the sample treated with lower concentration of 150 µg/mL. The pseudo-blue fluorescence color illustrates cell nuclei stained by DAPI.

To further evaluate the biodistribution of the internalized ICG inside the cells, the treated cells were imaged with our custom-built PAM imaging system. PAM images of the treated cells were acquired at the optical wavelength of 700 nm with an excitation energy of 40 nJ. The morphology of a single cell as well as the distribution of ICG was clearly observed on the PAM with high contrast (Figs. 2A–D). The PAM image contrast of the cells treated at concentration of 150 µg/mL was not significantly lower than that of the samples treated with ICG at 200 and 250 µg/mL ($N = 3$, $P > 0.05$). There were no cells observed on the PAM image obtained from the control group.

By using regions of interest (ROI) analysis, quantitative fluorescent signal and PAM signal amplitudes were measured and plotted, as shown in Figures 2E, 2F. Both fluorescent and PAM signal significantly increased at 24 hours post incubation with ICG. The quantitative fluorescent intensity panel (see Fig. 2E) exhibits that fluorescent signal of the sample incubated with ICG at a concentration of 200 µg/mL increased by 72-fold when compared to control group (fluorescent signal = 65.42 ± 8.14 a.u. for 200 µg/mL vs. 0.90 ± 0.28 a.u. for control). The fluorescent signal is reduced approximately 68% when the cells were incubated with ICG at a lower concentration of 150 µg/mL (fluorescent signal = 38.93 ± 7.80 a.u.). The quantitative PAM signal also shows that the PA signal of the sample incubated with ICG at 200 and 250 µg/mL significantly enhanced and exhibited 18-fold and 14-fold higher signal amplitudes than that of control (i.e. PA_{signal} = 181.01 ± 19.87 a.u. for 250 µg/mL and 140.76 ± 20.56 a.u. for 200 µg/mL vs. PA_{signal} = 9.94 ± 1.91 a.u. for control). Note that the PA signal decreased 2.3 times when the incubation concentration decreased from 250 µg/mL to 150 µg/mL (PA_{signal} = 80.27 ± 8.52 a.u. for 150 µg/mL).

To examine the degree of ICG released from the labeled cells, an evaluation of the biodegradability of ICG dye in the bioenvironment was implemented. The

cells were labeled with ICG and incubated for 24 hours, 48 hours, 72 hours, day 5, and day 7. Figure 2G shows the fluorescent signal measured from the inlet fluorescent images of the harvested cells. The signal was gradually reduced over time. The result shows that half-life of ICG inside the cells was estimated to be 72 hours post treatment.

In Vivo PAM Imaging Visualization of ARPE-19 Cells

Both organic and inorganic materials such as ICG or gold nanoparticles are often used as contrast agents to label stem cells to track the fate and viability of the cells after transplantation.[27,44–46] In this study, ICG was used to label ARPE-19 cells that were transplanted into the subretinal space in living rabbits. Subretinal injection of labeled cells into the subretinal space in the living rabbits was implemented because it is a common method for RPE cell therapy in ophthalmology. Then, a custom-built multimodal PAM and OCT system was performed to monitor the cell viability, migration, and dynamic changes over time after transplantation. The color fundus photograph pre-injection shows the major retinal vessels, choroidal vessels, and capillaries (Fig. 3A). At the subretinal

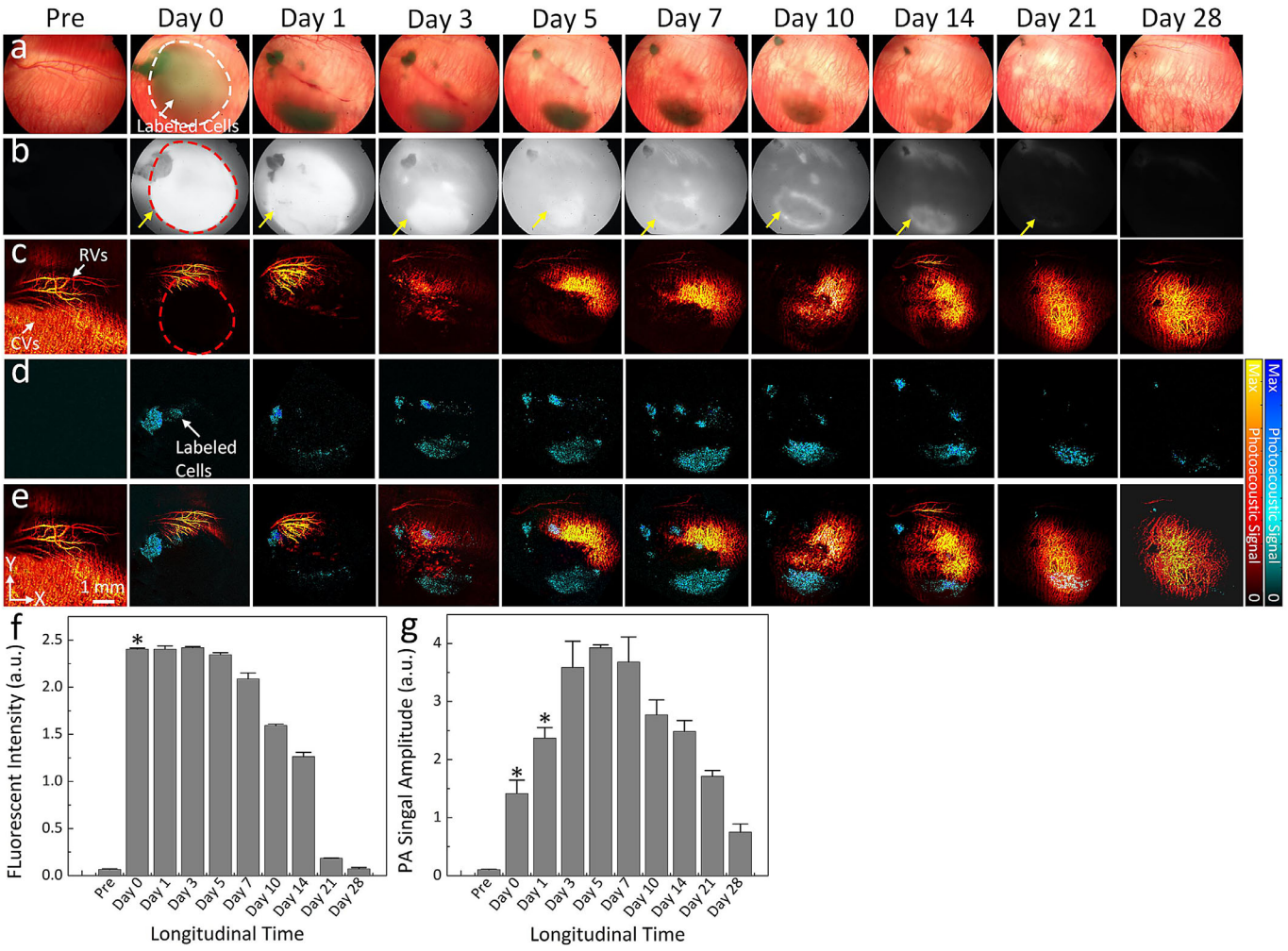

Figure 3. **Multimodal imaging visualization of ARPE-19 cells in living rabbits.** Color fundus photography, ICG, and PAM pre- and post-administration of ICG-RGD at different time points: 0 (immediately after injection), 1, 3, 5, 7, 10, 14, 21, and day 28. (**A, B**) Color fundus photography and fluorescence images before and after subretinal injection of ICG labeled-ARPE-19 cells into the subretinal space in the rabbit retina. These images were achieved longitudinally over a period of 28 days. The location of the cells after transplantation was clearly observed with strong fluorescence contrast (*red dotted circle*). The strongest fluorescence signal occurred from day 0 to day 5 post injection. (**D, E**) Maximum intensity projection (MIP) PAM images before and after cells transplantation acquired from two different wavelength of 578 and 700 nm. *White arrow* indicates the position of the transplanted cells. (**E**) Overlay PAM images acquired at 578 and 700 nm on the same imaging planes. Pseudo-cyan fluorescence color represents the cell viability as well as the migration pattern. (**F, G**) Quantitative measurement fluorescence signal intensity and PAM signal amplitudes, respectively.

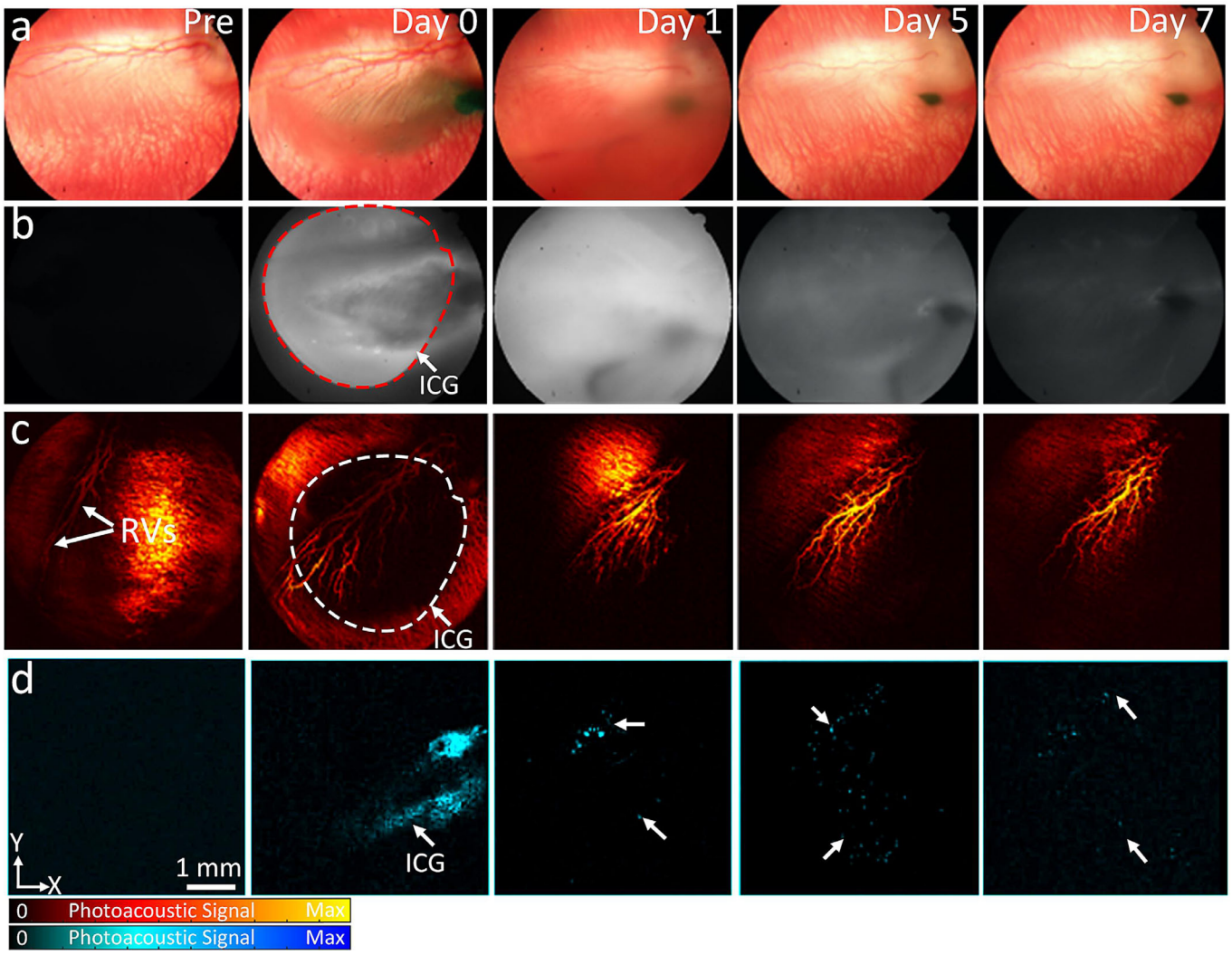

Figure 4. **In vivo evaluation of subretinal injection of ICG suspension solution.** Dynamic change of ICG in the subretinal space after subretinal injection was examined longitudinally. (**A, B**) color and fluorescence photographs of the rabbit retina before and after subretinal injection of ICG (20 µg/mL, 30 µL). Biodistribution of ICG in the subretinal space was clearly observed with strong fluorescent signal immediately after the injection (*red dotted circle*) and at day 1 post-injection. (**C, D**) Maximum intensity projection (MIP) PAM images obtained at 578 and 700 nm, respectively. *White arrows* indicate the distribution of ICG. The strongest PA signal was visible on the PAM acquired immediately post-injection. Then, the PAM signal rapidly reduced and was completely gone by day 7 post-injection.

injection location, the transplanted ICG-labeled cells were clearly observed at day 0 (white dotted circle) and significantly changed over time. Note that the transplanted cells were barely seen on the fundus color image at day 21 and day 28. The transplanted cells in the subretinal space were further monitored by ICG imaging (Fig. 3B). The ICG images illustrate the distribution, location, and migration pattern of the cells after delivery into the retina over time. The highest ICG image contrast was achieved at days 0, 1, 3, and 5 post injection and then the image contrast gradually reduced over time. This may be caused by the degradation of the internalized ICG dye. Minimal fluorescent signal was detected on the fluorescent image acquired at day 21 and completely disappeared in the image acquired at day 28. Figures 3C–E shows longitudinal observation of the ICG labeled ARPE-19 cells over a period of 28 days. In order to obtain the PAM image, 2 different optical wavelengths of 578 and 700 nm were selected as the excitation light source. The excitation wavelength of 578 nm was utilized to visualize the entire retinal vessel network due to strong optical absorption of hemoglobin (Hb) within retinal blood vessels at this wavelength. In addition, Hb has very low absorption of laser light at 700 nm, resulting in weak intrinsic PA signal at 700 nm. In contrast, ICG exhibits strong optical absorption at the wavelength of 700 nm, as shown in Figure 1A. Therefore, the

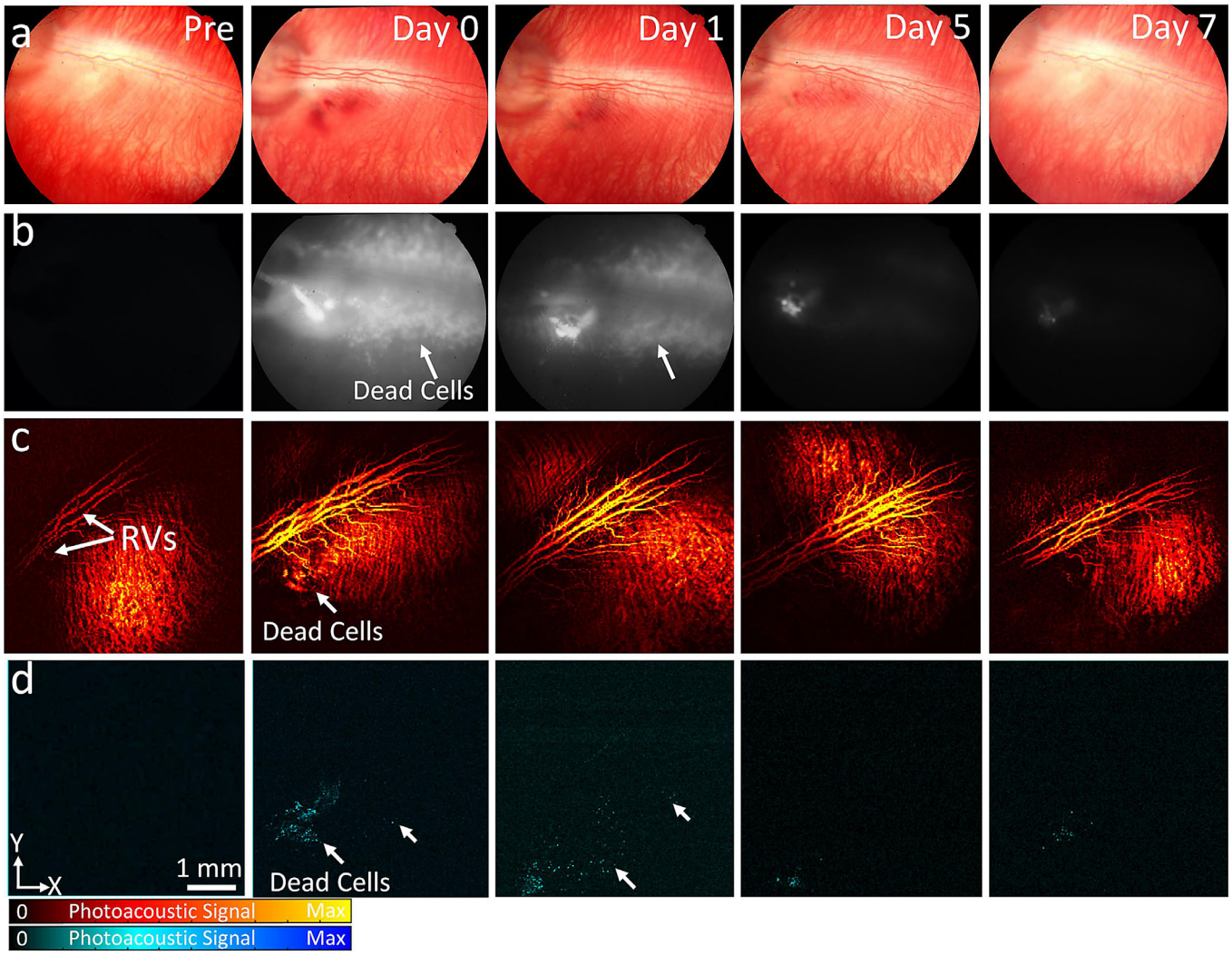

Figure 5. **In vivo visualization of dead ARPE-19 cells labeled with ICG.** (**A, B**) Color fundus and fluorescence photographs of the rabbit retina pre– and post-subretinal injection of 30 µL dead ICG labeled ARPE-19 cells at a density of 1×10^6 cells per millimeter. (**C, D**) MIP PAM images acquired at the excitation wavelengths of 578 and 700 nm, respectively. Dead cells were observed on the PAM image obtained at 700 nm and fluorescence images immediately and at day 1 post-injection (*white arrows*). Rapid reduction in the fluorescence and PAM signal was noted with the dead cells by 5 days with minimal signal by day 7 post-injection.

wavelength of 700 nm was used to detect transplanted cells. As shown in Figure 3D, there was minimal PA signal obtained before the injection of the cells and post injection of the cells at day 28. In contrast, strong PA signal was detected on the PAM images post-injection and achieved highest contrast at day 5. Figure 3E illustrates coregistration of the PAM image acquired at 578 and 700 nm on the same imaging planes. These images demonstrate the location and margin of the transplanted cells with good contrast and consistent with the color fundus and ICG images shown in Figures 3A and 3B. This result allows for distinguishing transplanted cells from the surrounding microvasculature. By using ROIs analysis, the fluorescent intensity and photoacoustic signal amplitudes on the ICG and PAM image before and after the injection were determined and displayed in Figures 3F and 3G. The fluorescent intensity was rapidly increased at day 0 post-injection and stable for up to 5 days. Then, the fluorescent signal was gradually decreased at day 7 to day 14 and completely gone at day 28 post-injection. Compared to the fluorescent signal before the injection, the fluorescent intensity was increased up to 37-fold from 0.07 $\pm$ 0.01 a.u. before injection to 2.41 $\pm$ 0.01 a.u. at day 0 post injection ($P < 0.001$). Interestingly, the peak fluorescent intensity was achieved from day 0 to day 5 and continued to achieve strong signal up to 14 days with the signal enhancement of 19-fold (fluorescent signal = 1.27 $\pm$ 0.04 a.u.). This result confirms that ICG could be a great fluorescent agent for labeling

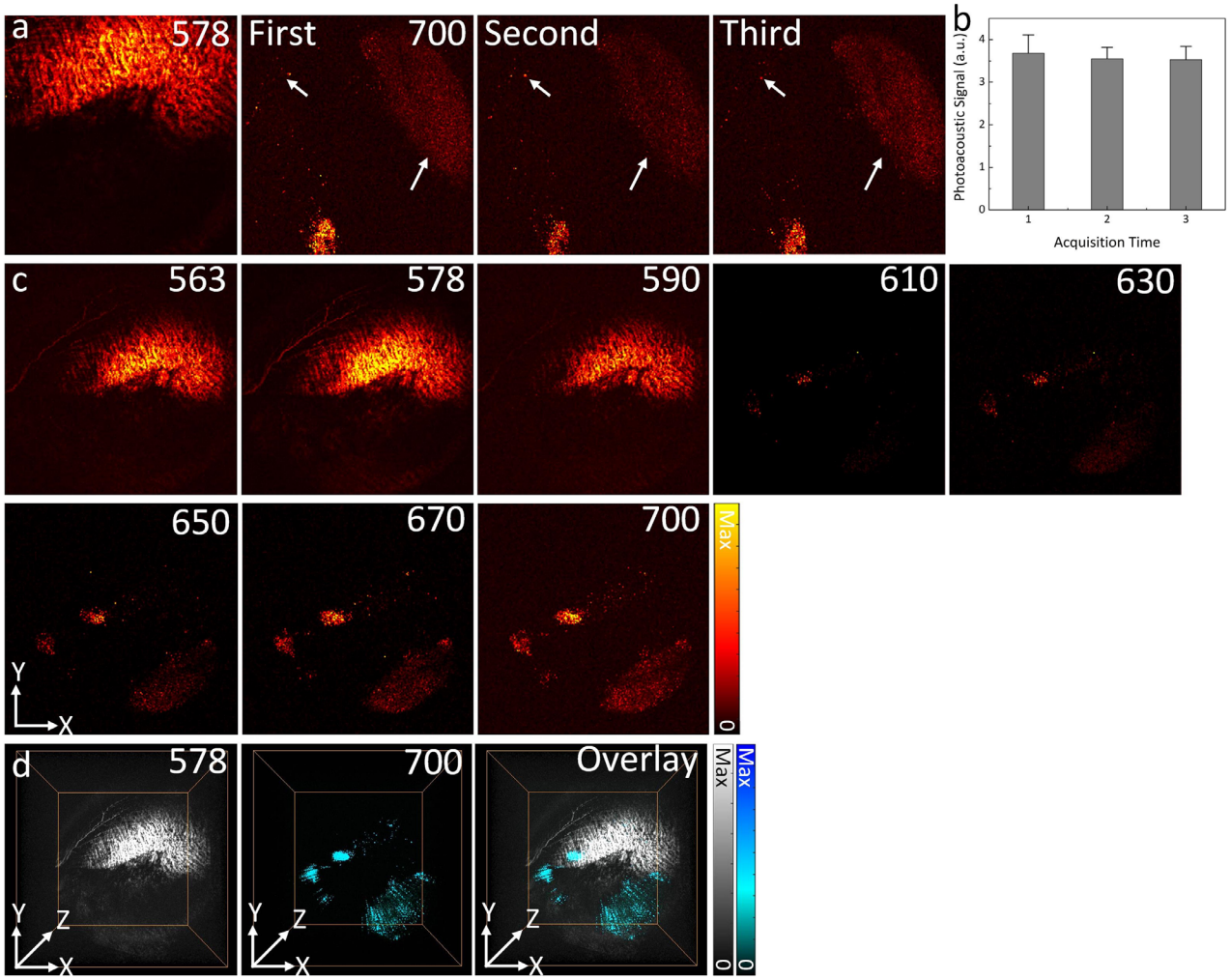

Figure 6. **In vivo photostability analysis and spectroscopic PAM image.** (**A**) MIP PAM images acquired at 578 nm and 700 nm at the same scanning areas. Noted that the PAM images at 700 nm were repeated three times. *White arrows* show the detected ARPE-19 cells. (**B**) A graph of PAM signal amplitudes isolated at the position of the detected cells. The quantitative PAM amplitudes were not significantly different among three scans and exhibited 4% fluctuation (i.e. 3.68 ± 0.43 a.u. for the first scan, and 3.53 ± 0.31 a.u. for the third scan, $P = 0.25 > 0.05$). (**C**) spectroscopic PAM images acquired at different wavelengths ranging from 563 nm to 700 nm. (**D**) The 3D rendering visualization of the PAM data.

and tracking stem cells longitudinally. Furthermore, quantitative measurement PA signal also revealed that PA signal significantly increased and reached a peak at day 5 post injection with the signal approximately 20-fold stronger than that of pre injection, as shown in Figure 3G (i.e. $PA_{signal} = 0.20 \pm 0.01$ a.u. for pre-injection vs. $PA_{signal} = 3.93 \pm 0.05$ a.u. for post-injection). The PA signals were then decreased over time and still achieved 3.84-fold higher signal at day 28 post injection ($PA_{signal} = 0.75 \pm 0.14$ a.u.; $P < 0.001$, $n = 3$). This significant signal enhancement permits for tracking the transplanted cells longitudinally as well as allows ICG to be an excellent contrast agent not only for fluorescent imaging, but also for PAM imaging. In contrast, in the control group which the animal received subretinal injection of ICG suspension solution at concentration of 20 µg/mL without labeling ARPE-19 cells, both fluorescent and PAM signals rapidly reduced at day 5 post subretinal injection and completely disappeared at day 7 (Fig. 4). This result can explain that the ICG dye released from the cells and uptake by the neighboring host cells upon disintegration may induce minimal PA and fluorescent signals.

To further evaluate the potential of dead ARPE-19 to be uptaken by local cells and visualized, we performed subretinal injection of dead ARPE-19 cells labeled with ICG. The results show that fluorescent and PAM signals were rapidly decreased at day 5 post-injection and completely gone at day 7, as shown in Figure 5. The data confirmed that administration of

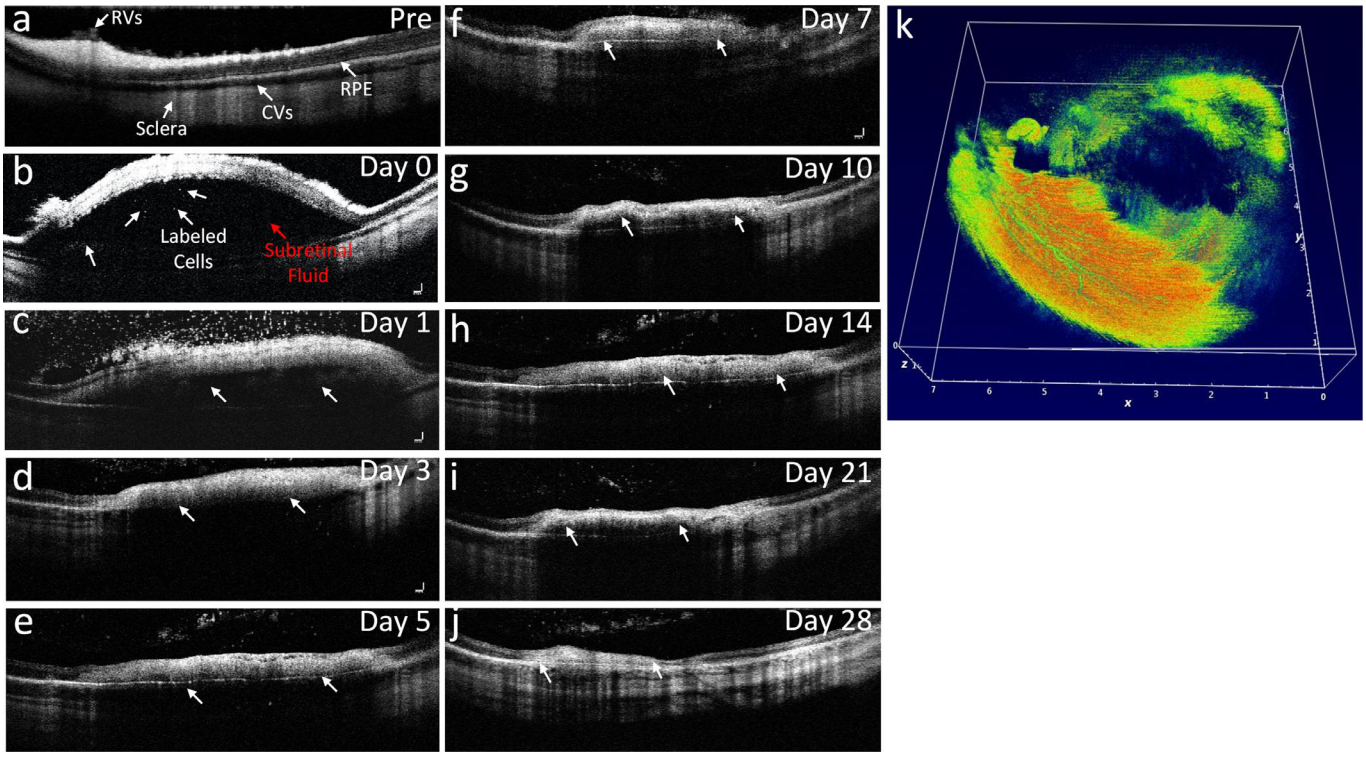

Figure 7. Optical coherence tomography (OCT) image of ARPE-19 cells. (**A–J**) Longitudinal B-scan OCT images obtained before and after cell transplantation. OCT image before the injection shows different intact retinal layers **A**, whereas localized retinal detachment was observed on the OCT image after injection **B**. Note that labeled cells were detected (*white arrows*) and randomly distributed in the subretinal space along with the accumulation of subretinal fluid. (**K**) The 3D OCT visualization. Encoded color shows different depths of retinal layers.

dead cells resulted in rapid decrease in PA and fluorescent signals by 5 to 7 days post-administration.

In order to examine any potential photobleaching during in vivo PAM experiments, the targeted area was scanned three time under the same laser energy and same scanning speed. To avoid the potential photobleaching effect cause by shorter wavelength, the PAM image was first acquired at 700 nm. This step was repeated for the second and the third time, and then switched to 578 nm and scanned for 3 more times. The data are displayed in Figure 6A. The PAM image contrast was not significantly varied between these images acquired both at 578 and 700 nm. The margin of cell distribution was clearly observed on the PAM image with great quality and high contrast. The quantitative PA signals (Fig. 6B) illustrate that the percentage of PA signal variation is approximately 4.1% among the 3 scans (i.e. 3.68 ± 0.43, 3.55 ± 0.27, and 3.53 ± 0.31 a.u. for the first, second, and third scans, respectively). Spectroscopic PAM image was implemented to evaluate any red shift of the internalized ICG in vivo by acquiring PAM images at different wavelengths ranging from 563 nm to 700 nm (Fig. 6B). The location of ICG-labeled ARPE-19 cells were clearly observed on the PAM acquired at 650 nm, 670, and 700 nm due to strong absorption of ICG. This is consistent with the absorption spectrum displayed in Figure 1A. In contrast, the cells were not observed on the PAM images obtained at lower wavelength of 563, 578, and 590 nm likely due to low absorption of ICG at these wavelengths. Figure 6C shows three-dimensional rendering of the PAM data acquired at 578 and 700 nm (left and middle sides) at day 5 post injection, and an overly PAM images (right side). Pseudo-cyan color indicates the position of the ICG labeled cells. Noted that the overlying image shows the distribution of the cells in 3D with high contrast and clearly distinguished from the surrounding retinal blood vessels (gray color).

Figures 7A–J show the cross-sectional B-scan OCT images obtained before and after transplanted cells into the subretinal space in the retina over time. The OCT image before injection shows different retinal layers such as retinal vessels (RVs), choroidal vessels (CVs), RPE, and sclera (Fig. 7A). These layers are intact and lay at different depths. Figure 7B shows the OCT image post subretinal delivery of the cells into the subretinal space. White arrows show the location of the cells in the subretinal space, whereas the red

arrow show the accumulate of subretinal fluid with the retina significantly detached. Retinal detachment was completely resolved at day 5 post injection and the transplanted cells were clearly observed. The cells demonstrated growth along the subretinal space (white arrows). Figure 6K demonstrates the 3D OCT image obtained at day 5 post injection. This image shows the retinal and choroidal vessels, and the location of the transplanted cells were in different layers (pseudo-depth color), resulting in improved visualization of the cell population after transplantation. Slit lamp biomicroscopy did not show significant anterior chamber cell or flare, vitritis, retinitis, retinal vasculitis, or subretinal infiltrate at any time post-injection.

In Vivo Immunohistochemistry Staining Analysis

To evaluate the fate and migration of the cells in the subretinal space after transplantation into the retina, a standard histological staining with H&E and immunohistochemistry staining analysis were implemented. Figures 8A and 8B show the H&E images of the sample harvested from control group (without cell transplantation) and experimental group at day 28 post treatment. The control H&E images (see Fig. 8A) showed the normal RPE morphology and pattern in the subretinal space. In contrast, the treated tissue showed abnormal RPE structure and pattern, indicating the growth of the transplanted cells (yellow arrows). To further assess the integration of the ARPE-19 cells in RPE layer, immunofluorescence staining was performed using RPE-65 antibody (Figs. 8C–L). RPE65-positive cells were clearly observed with aberrant morphology on the immunostaining image obtained from the treated group (Fig. 8K). Note that pseudo-red fluorescence color indicated the location and pattern of ARPE-19 cells. In contrast, the control group shows normal morphology of RPE cells (Fig. 8E). Blue fluorescence color is used to stain the cell nuclei (Figs. 8D, 8H). Figures 6F and 6L show the overlay brightfield images (Figs. 8C, 8G) and double staining fluorescence images. These images

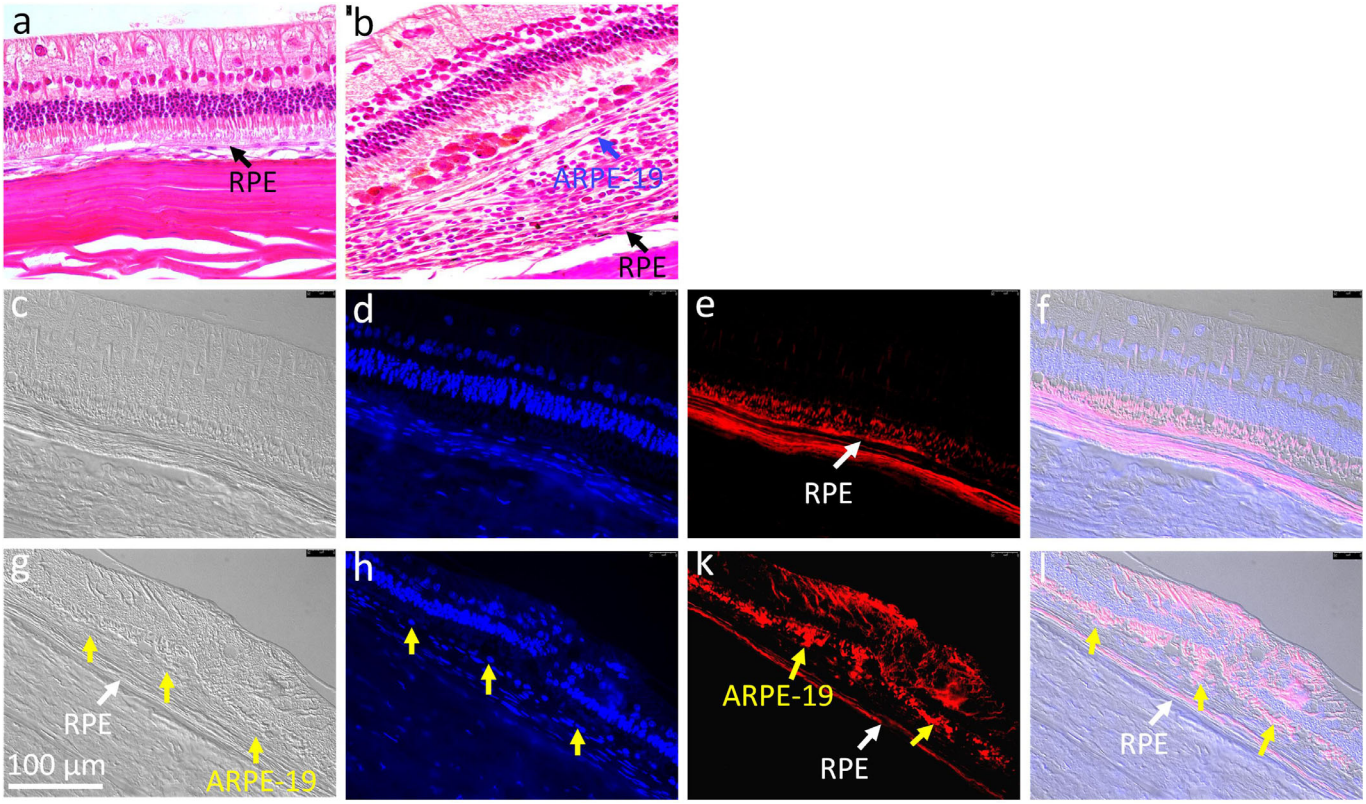

Figure 8. Histopathological and immunohistochemistry analysis. Hematoxylin and eosin (H&E) images of control group (**A**) and cell transplantation group (**B**). The transplanted ARPE-19 were clearly visualized in the subretinal space (*yellow arrow*). (**C–L**) immunofluorescence images of the control and cell transplanted tissues. Red fluorescence color indicates the RPE-65 positive. Blue color stained by DAPI. Bright-field images show the structure of retinal tissues. Images show the location ARPE-19 cells (*yellow arrows*) and native RPE cells (*white arrows*), which is consistent with OCT images.

show the loss of photoreceptor layer and the location of ARPE-19 cells within the subretinal space above the RPE layer, which is consistent with the B-scan OCT images, as shown in Figure 7. The challenge of this study is to achieve a monolayer of RPE cells after transplantation into the subretinal space and distinguish them from host RPE cells. We believed the proliferation rate of ARPE-19 cells is higher than that of host RPE cells, which causes the cells to form multiple layers in the subretinal space. To solve this problem, a primary RPE cell which has similar characteristics to host RPE or control the amount of transplanted cells to be injected into the subretinal space. Petrus-Reurer et al. have reported that a monolayer of RPE formed after injection of 5×10^4 cells into the subretinal space using hESC-derived RPE cells.[37]

Conclusions

In summary, the current study demonstrates that stem cells/progenitor cells (ARPE-19) can be successfully labeled with biocompatible FDA-approved ICG fluorescence dye, and cell location and integration was monitored in vivo using multimodal PAM, OCT, and fluorescence imaging. The experimental results showed that ICG at the highest tested concentration of approximately 200 to 250 µg/mL was not toxic to the cells. Therefore, higher PAM and fluorescence image contrast can be obtained by labeling cells with approximately 200 to 250 µg/mL concentration of ICG without a significant reduction in cell proliferation. Importantly, in vivo experimental data illustrated that the location and margin of the cells can be monitored longitudinally and distinguished from the surrounding retinal microvasculature. The cell viability was found to reduce gradually, and the cells can be tracked in real time using the OCT imaging system. These results indicate that ICG could serve as a great near infrared (NIR) contrast agent for labeling the cells for both fluorescent and PAM imaging. In addition, multimodal PAM and OCT could be a unique tool for tracking stem cells noninvasively, helping to improve understanding and evaluation the efficacy of cell-based therapies.

Acknowledgments

The authors thank Yuqing Chen and the Center for Advanced Models and Translational Sciences and Therapeutics (CAMTraST) at the University of Michigan Medical School for the generous donation of New Zealand rabbits, Thomas David for assistance with immunohistochemistry, David A. Antonetti for the generous donation of human ARPE-19 cells, and Phil Kish for supporting tissue culture facilities.

Supported by the National Eye Institute with Grant Number 1K08EY027458 (Y.M.P.) and Fight for Sight International Retinal Research Foundation grant number FFSGIA16002 (Y.M.P.). Also supported by unrestricted departmental support from Research to Prevent Blindness and the University of Michigan Department of Ophthalmology and Visual Sciences. This research utilized the Core Center for Vision Research financed by the National Eye Institute grant number P30 EY007003.

Disclosure: **V.P. Nguyen,** None; **Y. Li,** None; **J. Henry,** None; **T. Qian,** None; **W. Zhang,** None; **X. Wang,** None; **Y.M. Paulus,** None

References

1. Sharma R, Khristov V, Rising A, et al. Clinical-grade stem cell–derived retinal pigment epithelium patch rescues retinal degeneration in rodents and pigs. *Sci Transl Med*. 2019;11:eeat5580.
2. Jenq RR, Van den Brink MR. Allogeneic haematopoietic stem cell transplantation: individualized stem cell and immune therapy of cancer. *Nature Reviews Cancer*. 2010;10:213–221.
3. Huang Z, et al. Photoacoustic stimulation promotes the osteogenic differentiation of bone mesenchymal stem cells to enhance the repair of bone defect. *Scie Rep*. 2017;7:1–14.
4. Garber K. RIKEN suspends first clinical trial involving induced pluripotent stem cells. *Nat Biotechnol*. 2015;33(9):890–892.
5. Vagnozzi RJ, Maillet M, Sargent MA, et al. An acute immune response underlies the benefit of cardiac stem cell therapy. *Nature*. 2020;577:405–409.
6. Song MJ, Bharti K. Looking into the future: Using induced pluripotent stem cells to build two and three dimensional ocular tissue for cell therapy and disease modeling. *Brain Res*. 2016;1638:2–14.
7. da Cruz L, et al. Phase 1 clinical study of an embryonic stem cell–derived retinal pigment epithelium patch in age-related macular degeneration. *Nature Biotechnology*. 2018;36:328.
8. Strauss O. The retinal pigment epithelium in visual function. *Physiolog Rev*. 2005;85:845–881.
9. Hellinen L, et al. Characterization of artificially repigmented ARPE-19 retinal pigment epithelial cell model. *Sci Rep*. 2019;9:1–10.

10. Pelkonen L, et al. Melanin binding study of clinical drugs with cassette dosing and rapid equilibrium dialysis inserts. *Eur J Pharmaceutical Sci*. 2017;109:162–168.
11. Rimpelä A-K, et al. Implications of melanin binding in ocular drug delivery. *Advanced Drug Delivery Reviews*. 2018;126:23–43.
12. Jakubiak P, et al. Understanding molecular drivers of melanin binding to support rational design of small molecule ophthalmic drugs. *J Medicinal Chem*. 2018;61:10106–10115.
13. Larsson BS. Interaction between chemicals and melanin. *Pigment Cell Res*. 1993;6:127–133.
14. Robbie SJ, Lundh von Leithner P, Ju M, et al. Assessing a novel depot delivery strategy for non-invasive administration of VEGF/PDGF RTK inhibitors for ocular neovascular disease. *Invest Ophthalmol Vis Sci*. 2013;54:1490–1500.
15. Urtti A, Salminen L, Kujari H, Jäntti V. Effect of ocular pigmentation on pilocarpine pharmacology in the rabbit eye. II. Drug response. *Inter J Pharmaceutics*. 1984;19:53–61.
16. van Zeeburg EJ, Maaijwee KJ, Missotten TO, Heimann H, van Meurs JC. A free retinal pigment epithelium–choroid graft in patients with exudative age-related macular degeneration: results up to 7 years. *Am J Ophthalmol*. 2012;153:120–127.e122.
17. Celso CL, Fleming HE, Wu JW, et al. Live-animal tracking of individual haematopoietic stem/progenitor cells in their niche. *Nature*. 2009;457:92–96.
18. Schwartz SD, Regillo CD, Lam BL, et al. Human embryonic stem cell-derived retinal pigment epithelium in patients with age-related macular degeneration and Stargardt's macular dystrophy: follow-up of two open-label phase 1/2 studies. *Lancet*. 2015;385:509–516.
19. Schwartz SD, Hubschman JP, Heilwell G, et al. Embryonic stem cell trials for macular degeneration: a preliminary report. *Lancet*. 2012;379:713–720.
20. Reyes AP, Petrus-Reurer S, Antonsson L, et al. Xeno-free and defined human embryonic stem cell-derived retinal pigment epithelial cells functionally integrate in a large-eyed preclinical model. *Stem Cell Reports*. 2016;6:9–17.
21. Scarfe L, Brillant N, Kumar JD, et al. Preclinical imaging methods for assessing the safety and efficacy of regenerative medicine therapies. *NPJ Regen Med*. 2017;2:1–13.
22. Santiesteban DY, Kubelick K, Dhada KS, Dumani D, Suggs L, Emelianov S. Monitoring/imaging and regenerative agents for enhancing tissue engineering characterization and therapies. *Ann Biomed Eng*. 2016;44:750–772.
23. Naumova AV, Modo M, Moore A, Murry CE, Frank JA. Clinical imaging in regenerative medicine. *Nature Biotechnology*. 2014;32:804–818.
24. Carter M, Shieh J. In: *Guide to Research Techniques in Neuroscience* (Second Edition) (eds Carter Matt, Shieh Jennifer) 117–144. Camp Hill, PA: Academic Press; 2015.
25. Chehade M, Srivastava AK, Bulte JW. Co-registration of bioluminescence tomography, computed tomography, and magnetic resonance imaging for multimodal in vivo stem cell tracking. *Tomography*. 2016;2:158.
26. Dhada KS, Hernandez DS, Suggs LJ. In vivo photoacoustic tracking of mesenchymal stem cell viability. *ACS Nano*. 2019;13:7791–7799.
27. Donnelly EM, Kubelick KP, Dumani DS, Emelianov SY. Photoacoustic image-guided delivery of plasmonic-nanoparticle-labeled mesenchymal stem cells to the spinal cord. *Nano Letters*. 2018;18:6625–6632.
28. Nguyen VP, Li Y, Qian W, et al. Contrast agent enhanced multimodal photoacoustic microscopy and optical coherence tomography for imaging of rabbit choroidal and retinal vessels in vivo. *Sci Rep*. 2019;9:5945.
29. Kim J-W, Galanzha EI, Shashkov EV, Moon H-M, Zharov VP. Golden carbon nanotubes as multimodal photoacoustic and photothermal high-contrast molecular agents. *Nature Nanotechnology*. 2009;4:688–694.
30. de la Zerda A, Bodapati S, Teed R, et al. Family of enhanced photoacoustic imaging agents for high-sensitivity and multiplexing studies in living mice. *ACS Nano*. 2012;6:4694–4701.
31. Yang K, Zhu L, Nie L, et al. Visualization of protease activity in vivo using an activatable photoacoustic imaging probe based on CuS nanoparticles. *Theranostics*. 2014;4:134–141.
32. de la Zerda A, Liu Z, Bodapati S, et al. Ultrahigh sensitivity carbon nanotube agents for photoacoustic molecular imaging in living mice. *Nano Lett*. 2010;10:2168–2172.
33. Fu Q, Zhu R, Song J, Yang H, Chen X. Photoacoustic imaging: contrast agents and their biomedical applications. *Advanced Materials*. 2019;31:1805875.
34. Jathoul AP, Laufer J, Ogunlade O, et al. Deep in vivo photoacoustic imaging of mammalian tissues using a tyrosinase-based genetic reporter. *Nature Photonics*. 2015;9:239–246.
35. Jiang Y, Kumar Upputuri P, Xie C, et al. Broadband absorbing semiconducting polymer

nanoparticles for photoacoustic imaging in second near-infrared window. *Nano Lett*. 2017;17:4964–4969.
36. Kim C, Song KH, Gao F, Wang LV. Sentinel lymph nodes and lymphatic vessels: noninvasive dual-modality in vivo mapping by using indocyanine green in rats—volumetric spectroscopic photoacoustic imaging and planar fluorescence imaging. *Radiology*. 2010;255:442–450.
37. Petrus-Reurer S, Bartuma H, Aronsson M, et al. Integration of Subretinal Suspension Transplants of Human Embryonic Stem Cell-Derived Retinal Pigment Epithelial Cells in a Large-Eyed Model of Geographic Atrophy. *Invest Ophthalmol Vis Sci*. 2017;58:1314–1322.
38. Tian C, Zhang W, Mordovanakis A, Wang X, Paulus YM. Noninvasive chorioretinal imaging in living rabbits using integrated photoacoustic microscopy and optical coherence tomography. *Optics Express*. 2017;25:15947–15955.
39. Kuo T-R, Hovhannisyan VA, Chao Y-C, et al. Multiple Release Kinetics of Targeted Drug from Gold Nanorod Embedded Polyelectrolyte Conjugates Induced by Near-Infrared Laser Irradiation. *J Am Chem Soc*. 2010;132:14163–14171.
40. Tian C, Zhang W, Nguyen VP, Wang X, Paulus YM. Novel Photoacoustic Microscopy and Optical Coherence Tomography Dual-modality Chorioretinal Imaging in Living Rabbit Eyes. *J Vis Exp*. 2018:132;e57135.
41. Nguyen VP, Li Y, Zhang W, Wang X, Paulus YM. Multi-wavelength, en-face photoacoustic microscopy and optical coherence tomography imaging for early and selective detection of laser induced retinal vein occlusion. *Biomedical Optics Express*. 2018;9:5915–5938.
42. Shi H, Zhang Z, Wang X, et al. Inhibition of autophagy induces IL-1β release from ARPE-19 cells via ROS mediated NLRP3 inflammasome activation under high glucose stress. *Biochem Biophys Res Commun*. 2015;463:1071–1076.
43. Cardillo JA, Jorge R, Costa RA, et al. Experimental selective choriocapillaris photothrombosis using a modified indocyanine green formulation. *British Journal of Ophthalmology*. 2008;92:276–280.
44. Chen Y-S, Zhao Y, Yoon SJ, Gambhir SS, Emelianov S. Miniature gold nanorods for photoacoustic molecular imaging in the second near-infrared optical window. *Nature Nanotechnology*. 2019;14:465–472.
45. Sabapathy V, Mentam J, Jacob PM, Kumar S. Noninvasive optical imaging and in vivo cell tracking of indocyanine green labeled human stem cells transplanted at superficial or in-depth tissue of SCID mice. *Stem Cells International*. 2015;2015:606415.
46. Park JY, Han J, Jung HS, et al. Synthetic probes for in vitro purification and in vivo tracking of hepatocytes derived from human pluripotent stem cells. *Biomaterials*. 2019;222:119431.